05,13

Particularities of spin wave propagation in magnonic crystals with nonuniform magnetization distribution across the thickness

© V.K. Sakharov[1], Y.V. Khivintsev[1], G.M. Dudko[1], A.S. Dzhumaliev[1], S.L. Vysotskii[1], A.I. Stognij[2], Yu.A. Filimonov[1]

[1] Saratov Branch, Kotel'nikov Institute of Radio Engineering and Electronics, Russian Academy of Sciences, Saratov, Russia
[2] Scientific-practical materials research centre Institute of solid state physics and semiconductors, NAS, Minsk, Belarus

E-mail: valentin@sakharov.info

Received April 29, 2022
Revised April 29, 2022
Accepted May 12, 2022.

With the help of micromagnetic modeling, we considered particularities of dispersions and amplitude-frequency response of spin waves in a magnonic crystal (MC) formed by etching an array of grooves in the surface of yttrium iron garnet film having linear distribution of magnetization across the thickness from 1.7 kG at the upper surface till 2.02 kG at the bottom. For the geometry of surface magnetostatic spin waves (MSSW), it is shown that nonuniformity of magnetization distribution across the thickness leads to the appearance of frequency regions in the MC spectrum where MSSW propagation is unidirectional and, as the consequence, does not have Bragg resonances. It was also demonstrated that the MC spectrum is determined by the choice of surface used for the formation of the array of grooves.

Keywords: spin wave, micromagnetic modelling, film of yttrium iron garnet, magnonic crystal.

DOI: 10.21883/PSS.2022.09.54160.11HH

1. Introduction

Periodic magnetic structures — magnonic crystals (MC) [1] — are actively investigated both for studying the physics of wave processes and for possible application in magnonics [2–5]. The spectra of spin-wave excitations in MC differ significantly from the spectra in uniform media, in particular, they demonstrate the formation of forbidden bands in which spin waves (SW) cannot propagate. At the same time, certain attention is paid to the influence of various types of spatial nonuniformities on the forbidden bands formation [3–5]. In particular, the influence of the nonuniformity of the waveguide thickness [6] or irregularity of the structure periodicity [7,8] are studied. Also, some attention is paid to the study of the effect on the SW spectrum of the nonuniformity of the MC ground state caused by thermal gradients [9] or by demagnetization fields [10]. The purpose of this paper is to study the features of the spectrum formation and propagation of SW in MC based on magnetic films with a nonuniform distribution of magnetization ($4\pi M$) through the film thickness d.

Note that earlier [11] the spectrum of exchange spin waves (ESW) in a multilayer magnetic was theoretically studied taking into account the periodic modulation of all magnetic parameters of the material included in the Landau–Lifshitz equation, including $4\pi M$. In this paper, we study the spectrum and propagation of dipole-exchange SWs in MC formed by „etching" on one of the film surfaces of a periodic array of grooves by the method of micromagnetic simulation. In this case, a film of yttrium iron garnet (YIG) is studied with a $4\pi M$ linear change through the thickness from $4\pi M_b$ on the lower surface to $4\pi M_t$ on the upper ($4\pi M_b < 4\pi M_t$). Also note that the nonuniform distribution of $4\pi M$ through the thickness of YIG films can arise both due to the features of the film deposition technology leading to the formation of transition layers at the interface with the substrate [12,13], as well as can be formed purposefully with a given $4\pi M$ distribution through the thickness [14–19]. By choosing the nature of the $4\pi M$ distribution through the thickness, one can effectively excite ESW [16–19], as well as control the dispersion and effects of nonreciprocity of SW propagation [13–15,20,21]. In this paper, we study the effect of the noted features on the spectrum and propagation of SW in MC based on films with $4\pi M$ linear distribution through the thickness. In this case, we study SW propagation in the Damon–Eshbach configuration of magnetostatic surface waves (MSSW) [22] when the wave vector **k** of the spin wave is directed perpendicular to the tangential external magnetic field **H**. This choice is due to the fact that for MSSW, in contrast to the magnetostatic backward volume waves (MSBVW) propagating along the field, the $4\pi M$ thickness nonuniformity leads to the nonreciprocity of the spectrum, and also enhances the hybridization of MSSW with ESW [23].

2. Studied structure and calculation method

Fig. 1 shows the studied structures and „geometry" of the problem. The studied MCs „are made" from the

YIG film shown in Fig. 1, *a*. The magnetization in the film varied linearly through the thickness $d = 780$ nm from $4\pi M_b = 1700$ G at the boundary $z = 0$ to $4\pi M_t = 2020$ G at $z = d$. Note that the change in $4\pi M$ values through the thickness by $4\pi\Delta M = 320$ Oe can be implemented for YIG films of both micron [18] and submicron [13] thicknesses. The exchange constant D_{ex}, the gyromagnetic ratio γ, and the MSSW damping parameter α were assumed to be characteristic for YIG [5]: $D_{ex} = 3.1 \cdot 10^{-9}$ Oe $\cdot$ cm^2, $\gamma = 2.8$ MHz/Oe and $\alpha = 10^{-3}$. Along the axis, Ox the film was 520 μm long, and along the axis Oy, it was infinite. At the same time, to reduce the influence of MSSW reflections from the ends of the film, the damping linearly increased towards the ends up to the values $\alpha = 1$ in „damp“ sections of the film that were 34 μm long (see Fig. 1).

Fig. 1, *b* and *c* show the MCs under study, for which the groove width w and the period Λ were: $w = 18\,\mu$m and $\Lambda = 36\,\mu$m. MCs with groove depth $b = 60$ and 120 nm were considered. The magnonic crystal in Fig. 1, *b* (further MC1) was formed on the surface $z = d$ with magnetization $4\pi M_t(z = d) = 2020$ G. The magnonic crystal in Fig. 1, *c* (further MC2) was formed at the film boundary $z = 0$, where $4\pi M_b(z = 0) = 1700$ G. The external magnetic field H having value $H = 320$ Oe was directed along the axis Oy coinciding with the direction of the grooves. The SWs propagated along the axis Ox, which corresponds to the MSSW configuration.

Micromagnetic modeling was carried out using the freely distributed program Object Oriented Micromagnetic Framework (OOMMF) [24], and post-processing of the obtained data was executed similar to [25]. The lattice cell size was $dx \times dy \times dz = 80 \times 15 \times 15$ nm. Periodic boundary conditions were applied along the axis Oy. Note that for the chosen cell dimension across the film thickness dz, the YIG film with $d = 780$ nm consists of $N_L = 52$ layers. Each i-th $(1 \le i \le 52)$ layer has the thickness $dz = 15$ nm and magnetization $4\pi M_i$

$$4\pi M_i = 4\pi M_b + (i-1) \cdot \frac{4\pi\Delta M}{d - dz}\, dz. \qquad (1)$$

MSSW and ESW were excited by a field pulse directed along the axis Oz:

$$h_{\text{in}} = A\,\text{sinc}(2\pi f_c[t - t_0]), \qquad (2)$$

where $A = 100$ A/m is pulse amplitude; $f_c = 5$ GHz is frequency; t is time; $t_0 = 50$ ns is time offset. This pulse was applied to a region $\xi = 1\,\mu$m wide, located at the center of the sample ($x_{\text{in}} = 260\,\mu$m) and considered as an input antenna. As output antennas the sections of the film „out$L$“ and „out$R$“ $\xi = 1\,\mu$m wide, located at $x_{\text{out}L} = 44\,\mu$m and $x_{\text{out}R} = 476\,\mu$m were considered (see Fig. 1).

The obtained distributions $4\pi M(x, y, z, t_i)$ over the entire structure were stored every $t_i = 100$ ps, and the averaged signal (full field) under the input antenna $h_{\text{in}}(t_i)$ and two output antennas $h_{\text{out}L}(t_i)$, $h_{\text{out}R}(t_i)$ — every $t_i = 25$ ps. Further, to plot maps of the dispersion characteristics

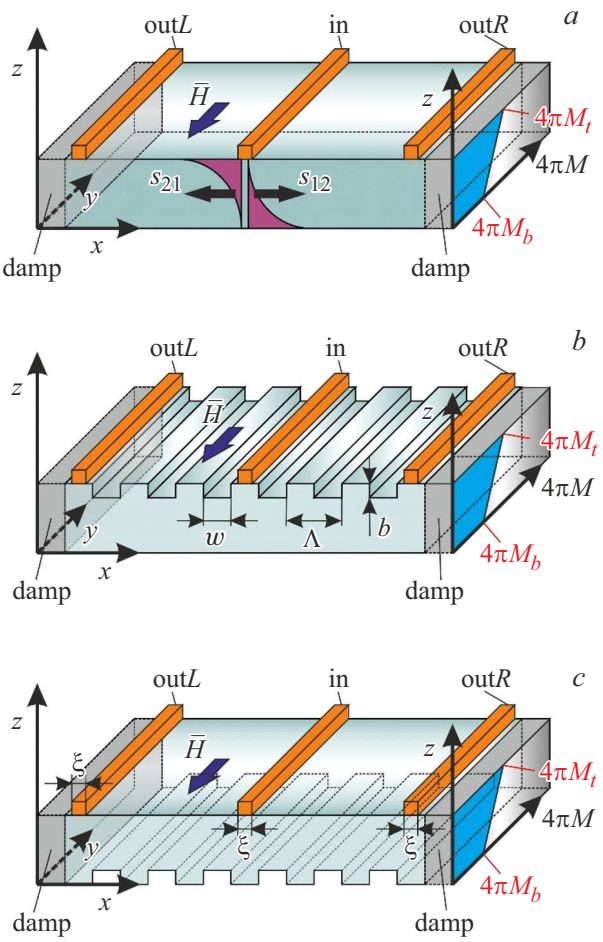

Figure 1. Schematic representation of the structures under study: YIG film with a linear distribution of $4\pi M$ through the thickness (*a*) and MC based on this film (*b, c*). SW damping in the regions „damp“ grows linearly from $\alpha = 10^{-3}$ to $\alpha = 1$; „in“, „out$L$“ and „out$R$“ indicate the position of the input and output antennas. Below the input antenna on (*a*) the schematic distributions through the film thickness of MSSW amplitudes propagating in the direction of the antennas „out$L$“ and „out$R$“ are given.

$f = f(k)$, the two-dimensional Fourier transform in time and space from the set $4\pi M(x, t_i)$ was used (averaging was carried out over y and z).

To analyze the MSSW propagation in the structures shown in Fig. 1, the amplitude-frequency characteristics (AFC) of „delay lines“ formed by „input“ and „output“ („out$L$“ and „out$R$“) antennas were calculated. AFC of the transmission coefficients $S_{12}(f)$ (from „output“out$R$“) and $S_{21}(f)$ (from output „out$L$“) were determined by the relations

$$S_{21} = 20\lg\big(FFT[h_{\text{out}L}]/FFT[h_{\text{in}}]\big), \qquad (3)$$

$$S_{12} = 20\lg\big(FFT[h_{\text{out}R}]/FFT[h_{\text{in}}]\big), \qquad (4)$$

where $FFT[h_{\text{in}}]$, $FFT[h_{\text{out}L}]$ and $FFT[h_{\text{out}R}]$ — Fourier transform amplitudes from time realizations $h_{\text{in}}(t)$, $h_{\text{out}L}(t)$

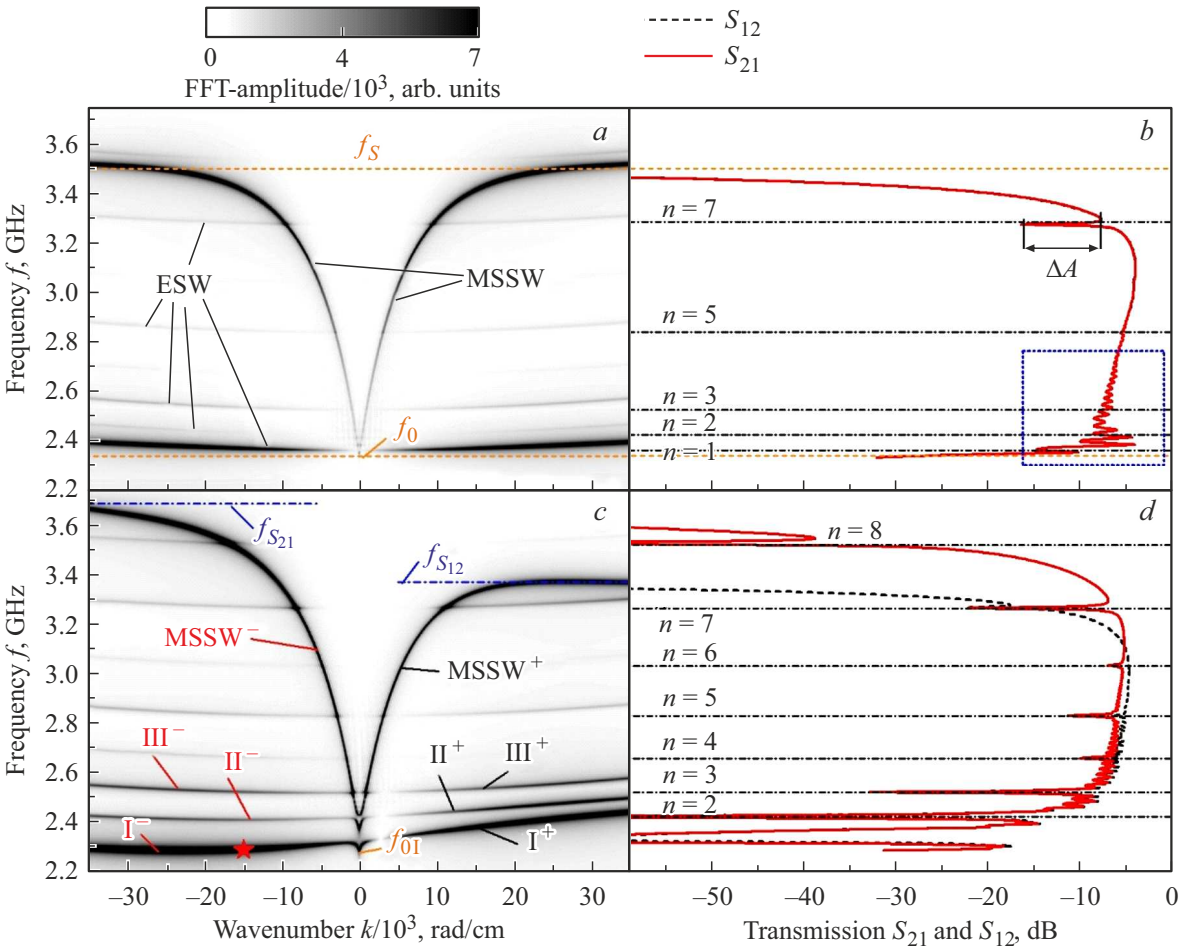

Figure 2. Dispersion characteristics (a, c) and AFC (b, d) for MSSW and ESW propagating in the YIG film with $4\pi M = 1860$ G (a, b) and with distribution $4\pi M(z)$ of the form (1) (c, d). The solid curves on (b, d) correspond to S_{21}, the dashed curves correspond to S_{12}. Horizontal dash-dotted lines on (b, d) show the positions of the DER frequencies, which practically coincide with the cutoff frequencies of the ESW modes of the corresponding numbers n.

and $h_{outR}(t)$, respectively. Besides, the calculations take into account only the amplitudes $S(f) > -60$ dB, which are typical for experiments with delay lines on MSSW [13].

Note that equations (3) and (4) use the values $h_{in}(t)$, $h_{outL}(t)$ and $h_{outR}(t)$ obtained by averaging through the entire sample thickness in the antenna region. This allows us to exclude from consideration the contribution to AFC from the nonreciprocity of excitation and reception of MSSW propagating from the input antenna in the direction of the output antennas „out$L$“ and „out$R$“. In no way the origin of such nonreciprocity is related to the $4\pi M(z)$ distribution and is due to the fact that the MSSW amplitude (UHF component of the magnetization $m(z)$) has the maximum near the film surface, the normal $\mathbf{n}$ to which coincides with the direction of the vector $\mathbf{k} \times \mathbf{M}$ [22], i.e., for $k > 0$, MSSW is localized at the boundary $z = 0$, and for $k < 0$ — at the boundary $z = d$ (see the distribution of MSSW amplitudes under the input antenna in Fig. 1, a). As a result, for the case $k > 0$ and for the case $k < 0$, the MSSW amplitude and the antenna field h ($h = h_{in}$, h_{outL}, h_{outR}) located on the surface $z = d$ have a different overlap integral $I \sim \int_0^d h \cdot m(z)dz$, the value of which characterizes the efficiency of MSSW excitation and reception by antenna. Averaging the values of the fields $h_{in}(t)$, $h_{outL}(t)$ and $h_{outR}(t)$ through the thickness, we, thus, exclude the nonreciprocity in AFC associated with the difference in the overlap integrals. Note that in the case of films with $4\pi M(z) = \text{const}$, the amplitudes of $S_{12}(f)$ and $S_{21}(f)$ waves transmitted to the output antennas coincide (see Fig. 2, b). As a result, all the differences between the $S_{12}(f)$ and $S_{21}(f)$ curves calculated using (3) and (4) will be related to the influence of the nonuniform distribution $4\pi M(z)$ in film.

3. Results and discussion

It is convenient to discuss the features caused by a linear change of the magnetization through the thickness in AFC and the dispersion curves of MSSW propagating in MC1 and MC2 in comparison with the case of MC with similar parameters, but with a constant magnetization through the thickness. To do this, we will use the case

of the structures shown in Fig. 1, based on the YIG film with magnetization constant through the thickness and equal to the averaged value $4\pi M = 1860$ G. At the same time, in Section 3.1 the dispersions and AFCs for films with uniform and nonuniform distributions of magnetization are compared, and in Section 3.2 the characteristics of MCs based on films with uniform and nonuniform distributions of magnetization are compared.

3.1. Uniform and nonuniform YIG films without periodic relief

Fig. 2 shows the dispersion characteristics $f(k)$ and the frequency response $S_{12}(f)$, $S_{21}(f)$ calculated for the cases of MSSW propagation in the YIG films with uniform $4\pi M(z) = 1860$ G (Fig. 2, *a, b*) and linear (Fig. 2, *c, d*) magnetization profile. The black-and-white scale for the dependences $f(k)$ characterizes the intensity of SW excitation by the field (2). In the obtained dependences $f(k)$ one can distinguish both mainly dipole (MSSW) and predominantly exchange modes (ESW). In maps $f(k)$, the intensity of the ESW lines with an integer number of half-waves $\lambda/2$ through the thickness is substantially less than the ESW modes with odd numbers n (see Fig. 2, *a* and *c*). This is especially noticeable for the film with $4\pi M(z) = 1860$ G, where the ESW modes of even numbers n and wave numbers $|k| < 10^4\,\mathrm{cm}^{-1}$ are practically not excited (Fig. 2, *a*). Such a behavior of the intensities of the ESW modes of even and odd numbers n reflects the behavior of the overlap integral $I_n \sim \int_0^d h_{\text{in}} \cdot m_n(z)dz$ between the exciting field h_{in} and the amplitude of UHF component of the magnetization $m_n(z)$ of the n-th ESW mode. In the film with a linear change of $4\pi M(z)$, the distribution $m_n(z)$ differs from the harmonic one [18], and effective excitation of the ESW modes of both even and odd numbers n by the Schlomann mechanism is implemented [26].

The so-called dipole-exchange resonances (DERs) are formed at the intersections of the dispersion curves of MSSW and ESW, leading to the repulsion of the dispersion curves [27]. At the same time, in AFC at DER frequencies (the position of such frequencies is shown by dash-dotted horizontal lines in Fig. 2, *b, d*), there is [28] an increase of the losses in the form of narrow-frequency „dips“ by ΔA (see Fig. 2, *b*).

Let us now discuss the most striking differences in the spectra $f(k)$ and AFC of the films (Fig. 2) associated with the behavior of $4\pi M(z)$ changing according to (1). Note that the range of wave numbers k in Fig. 2 is limited by the values $|k| \le 3.5 \cdot 10^4\,\mathrm{cm}^{-1}$, which are most effectively excited by microstrip antennas $\xi = 1\,\mu$m wide [29]. Comparison of the $f(k)$ dependences in Fig. 2, *a* and Fig. 2, *c* shows that in the films with linear behavior $4\pi M(z)$, the dispersion properties are nonreciprocal. The nonreciprocity manifests itself most clearly in the high-frequency part of the MSSW$^{\pm}$ dispersion curves, as well as the first three modes of the film marked I$^{\pm}$, II$^{\pm}$, III$^{\pm}$ in Fig. 2, *c*. In Fig. 2, *c*, the dispersion curve I$^-$ at $|k_{\max}| \approx 1200\,\mathrm{cm}^{-1}$ reaches its maximum value $f_{\text{I}^-}^{\max} \approx 2.325$ GHz and with further increasing $|k|$ takes a negative slope. For $k < -14800\,\mathrm{cm}^{-1}$ (marked with an asterisk in Fig. 2, *c*), the I$^-$ mode drops to $F_1^{\text{int}*} \approx 2.293$ GHz below the long-wavelength limit [22] of the spectrum $f_{0I} \approx 2.298$ GHz, which differs from the expected limit $f_{0b} = \sqrt{f_H^2 + f_H f_{mb}} \approx 2.251$ GHz (where $f_H = \gamma H$, $f_{mb} = \gamma 4\pi M_b$) for $4\pi M_b = 1700$ G. Moreover, the solutions for MSSW with wave numbers $k > 0$ (I$^+$ branch) at frequencies $[F_1^{int*}, f_{0\text{I}}]$ are absent, which corresponds to the unidirectional propagation of the I$^-$ mode. The I$^+$ mode is characterized by the unidirectionality in the frequency range $[f_{\text{I}^-}^{\max}, f_{0\text{II}}]$, where $f_{0\text{II}} \approx 2.385$ GHz is the frequency of the long-wavelength limit for the next branch II$^{\pm}$, which differs from the expected limit $f_{0t} = \sqrt{f_H^2 + f_H f_{mt}} \approx 2.251$ GHz (where $f_{mt} \approx \gamma 4\pi M_t$) for $4\pi M_t = 2020$ G. In the upper part of the spectrum, MSSW propagation is unidirectional in the frequency range from $f_{S_{12}} \approx 3.378$ GHz to $f_{S_{21}} \approx 3.673$ GHz. In this case, the frequency $f_{S_{21}}$ with an accuracy of $\approx 1\%$ coincides with the short-wavelength limit of the spectrum of dipole MSSW [22] $f_{st} = f_H + 0.5 \cdot f_{mt} \approx 3.72$ GHz in the film with magnetization $4\pi M_t = 2020$ G. The frequency $f_{S_{12}}$ exceeds by ≈ 0.11 GHz the short-wavelength limit of the MSSW spectrum $f_{st} \approx 3.27$ GHz in the film with $4\pi M_b = 1700$ G.

Note that within the framework of the approach used to plot $f(k)$ dispersion curves, the dissipation leads to „broadening“ of dispersion curves in the phase (f, k) space. For example, for the I$^-$ mode, the width of the dispersion curve in Fig. 2, *c* is comparable to the existence band of the mode itself. The $f(k)$ dispersion curves can be calculated without taking into account losses using the approach in [20], in which the film is represented as a multilayer exchange-coupled structure. In this case, for a given number of layers N_L, the magnetization of the i-th layer $4\pi M_i$ is determined from (1), and the interlayer exchange parameter $A_{i,i+1}$ is defined by relation [20]:

$$A_{i,i+1} = \frac{D_{ex} M_i}{dz}. \tag{5}$$

Fig. 3 shows the results of dispersion calculation according to [20] for the used parameters for the film with a linear change of $4\pi M(z)$. Fig. 3, *b* shows the dispersions calculated for the interval of wave numbers corresponding to Fig. 2, *a, c*, and Fig. 3, *a* — for wave numbers $|k| \le 10^5\,\mathrm{cm}^{-1}$. It can be seen that the nature of the $f(k)$ dependences in Figs 2 and 3 is the same. The shading in Fig. 3, *b* shows the regions 1–3, in which SW propagation is unidirectional in the range of wave numbers $|k| \le 3.5 \cdot 10^4\,\mathrm{cm}^{-1}$. However, when SW with $|k| \ge 10^5\,\mathrm{cm}^{-1}$ is taken into account, the unidirectionality disappears (Fig. 3, *a*).

Note that the character of the dispersion of the I$^-$ mode, as well as of the II$^-$, III$^-$ modes in Fig. 2, *c* and Fig. 3, *b* is similar to the behavior of dipole „internal“ MSSW in a

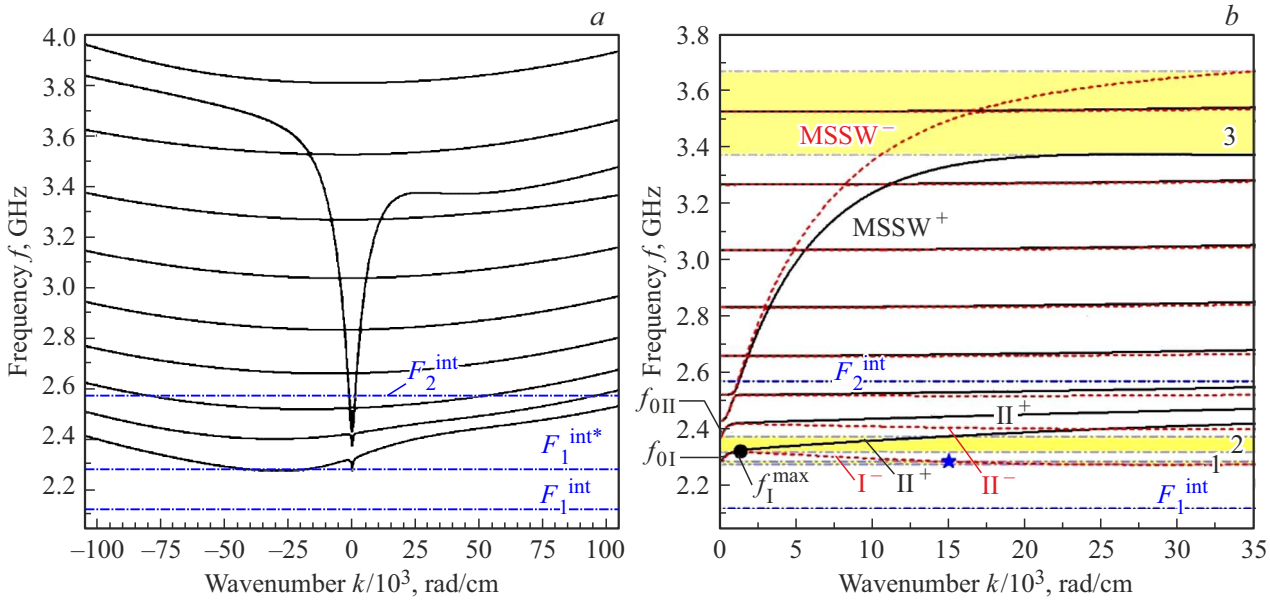

Figure 3. Dispersion curves of MSSW propagating in the YIG film with a linear distribution of magnetization through the thickness, calculated using the model of a multilayer exchange-coupled film. The dotted lines show the curves for the direction of propagation corresponding to $k < 0$, the solid curves — for $k > 0$. The horizontal dash-dotted lines show the position of the „internal“ MSSW $F_{1,2}^{int}$ calculated using relation (5) taken from [21] for the case of a two-layer film with layer magnetization $4\pi M_b = 1700$ G and $4\pi M_t = 2020$ G.

two-layer structure [21]. The horizontal dash-dotted lines in Fig. 3 show the frequencies $F_{1,2}^{int}$ corresponding to the short-wavelength limits of dipole „internal“ MSSW in a two-layer structure composed of films with a magnetization of $4\pi M_b = 1700$ G and $4\pi M_t = 2020$ G calculated using expression [21]:

$$F_{1,2}^{int} = \pm\frac{\Delta f_m}{4} + \sqrt{\left(\frac{\Delta f_m}{4}\right)^2 + \frac{f_{0t}^2 + f_{0b}^2}{2}}, \qquad (6)$$

where $\Delta f_m = \gamma 4\pi(M_t - M_b)$. It can be seen that in the frequency range F_2^{int}, the dispersion curves I$^+$, II$^+$, III$^+$ change their form due to the dipole interaction. The minimum frequency for the dispersion curve I$^-$, which is marked in Fig. 3, *b* by the horizontal dash-dotted line F_1^{int*}, differs markedly from the estimate F_1^{int}, obtained using (6). It is obvious that such a difference is associated with the film representation in [20] as a structure of $N_L = 52$ layers, while the magnetization of adjacent layers differs by $4\pi\Delta M \approx 6.27$ G.

The results of transmission spectra calculations for MSSW $S_{12}(f)$ and $S_{21}(f)$ in the studied films are shown in Fig. 2, *b, d*. It can be seen that the „valve“ effect in the film with the linear distribution $4\pi M(z)$ for the chosen distance between the antennas 216 μm appears only in the frequency band $[f_{S_{12}}, f_{S_{21}}]$, which is marked in Fig. 3 with shading as area 3. For the regions marked by shading 1 and 2 in the $f(k)$ spectrum in Fig. 3, *b*, unidirectionality in AFC does not manifest itself despite a significant difference in the nature of the dispersion of modes I$^\pm$, II$^\pm$, III$^\pm$. This is explained by the fact that all differences in the dispersion occur in the short-wavelength part of the spectrum, while for $|k| < 1200$ cm^{-1}, which determine AFC level, the differences in the character of the dispersion are insignificant (see. Fig. 3, *b*).

Besides, the linear nature of $4\pi M(z)$ distribution through the film thickness significantly enhances the effect of the DER on the shape of AFC of MSSW, see Fig. 2, *b, d*. From AFC comparison in Fig. 2, *b, d* it can be seen that the depth of dips ΔA in the film with nonuniform distribution $4\pi M(z)$ increases significantly. In this case, in contrast to the case of uniform films [28], the minimum values of ΔA are reached not in the long-wavelength part of the MSSW spectrum (see also Fig. 2, *b*), but occur in the central part of AFC (see Fig. 2, *d*). Besides, in AFC at the frequencies of some DERs ($n = 4-7$) the damping ΔA on the curves $S_{12}(f)$ and $S_{21}(f)$ is non-identical (non-reciprocal), since the non-reciprocity $f(k)$ is also expressed in different widths of exchange gaps.

3.2. Magnonic crystals

The results of calculation of dependences $f(k)$, $S_{21}(f)$ and $S_{12}(f)$ for MC based on a uniform film with $4\pi M = 1860$ G and for structures MC1, MC2 based on a film with nonuniform $4\pi M(z)$ distribution for the case of groove depth $b = 60$ nm are shown in Fig. 4.

First of all, note qualitatively identical changes in the dependences $f(k)$, $S_{21}(f)$, and $S_{12}(f)$ for MC based on films with both uniform and nonuniform distribution $4\pi M(z)$. It can be seen from Fig. 4 that reflections from the periodic lattice lead to the appearance in the $f(k)$

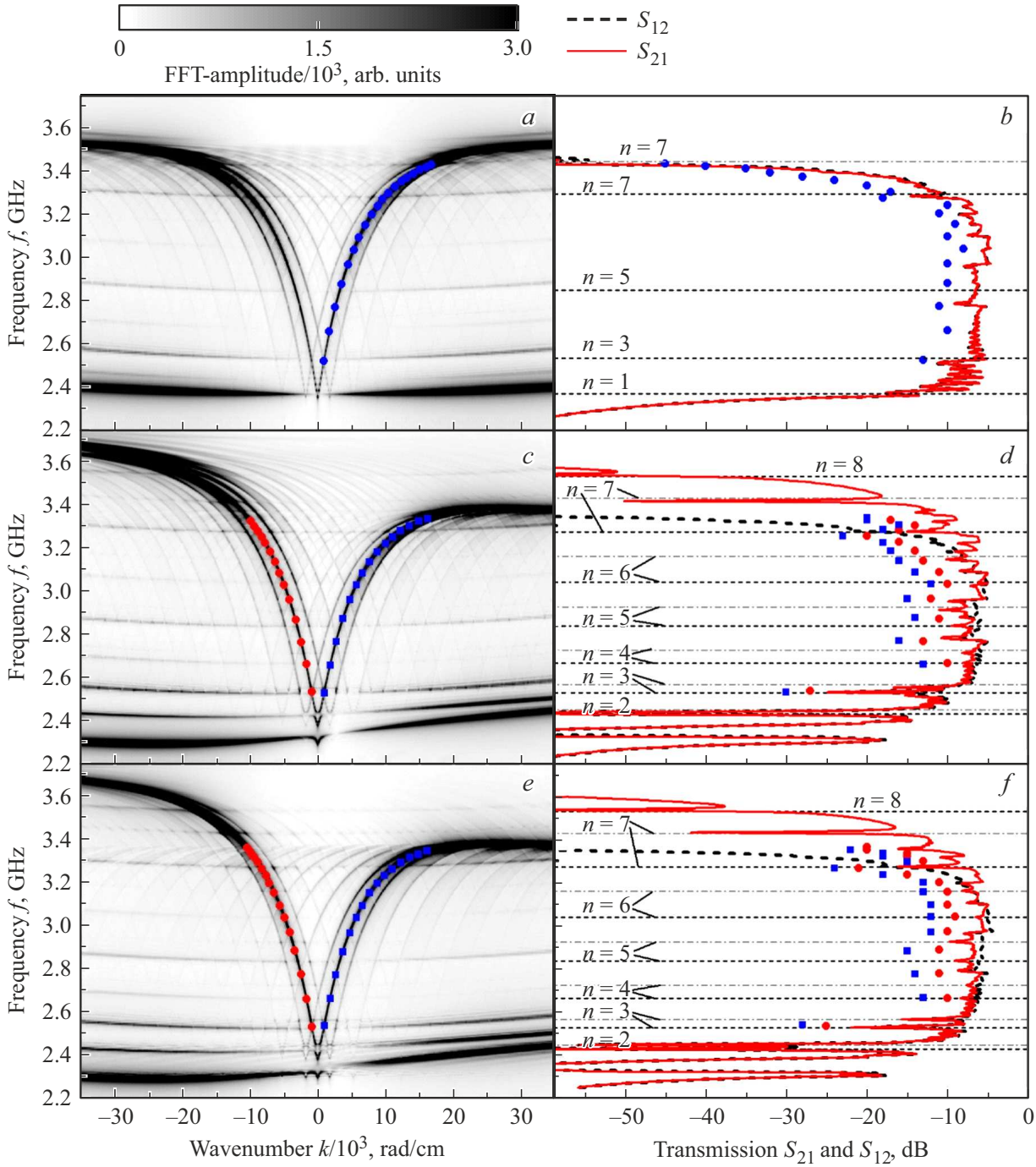

Figure 4. Dispersion characteristics (a, c, e) and AFC (b, d, f) for MSSW and ESW propagating in MC based on uniform YIG film with $4\pi M = 1860$ G and in the structures MC1 (c, d) and MC2 (e, f). The case of groove depth $b = 60$ nm. The solid curves on (b, d, f) correspond to S_{21}, the dashed curves to S_{12}. The horizontal dotted and dash-dotted lines on (b, d, f) show the positions of the DER frequencies with the corresponding numbers. The dots show the positions of the Bragg resonances.

spectrum of lattice of direct and reverse dispersion branches replicated along the wavenumber axis by $\pm 2\pi N/\Lambda$ (where $N = 1, 2, 3, \ldots$). The frequencies f^B, where the dispersion curves of „incident“ and „reflected“ SWs intersect, correspond to the generalized Bragg resonances (BR) [30]:

$$k_1(f^B) + k_2(f^B) = 2\pi N/\Lambda, \qquad (7)$$

where $k_{1,2}$ are wave numbers of incident and reflected MSSWs, N is the number of BR. At frequencies f^B, „forbidden“ bands are formed in the $f(k)$ spectrum, and ΔA dips (non-transmission regions) are formed in the AFC. As the groove depth b increases, the ΔA values at the frequencies f^B increase. Besides, the modulation of the film thickness d, caused by the grooves, leads to the appearance

of an additional DER grid associated with the appearance of ESW modes in the sections of the structure with a thickness of $d^* = d - b$ [31].

Let us now discuss the features in the MC spectrum related to the linear dependence of the film magnetization through the thickness of type (1). First of all, let's pay attention to the frequencies where the SW propagation in the film has a unidirectional nature — see frequency bands 1, 2, 3 marked by shading in Fig. 3, *a*. It can be seen from Fig. 4 that at frequencies $f_{S_{12}} < f < f_{S_{21}}$ (3.38−3.67 GHz) there are no BRs, since at these frequencies there is no reflection for MSSW.

One can see that periodic lattices of grooves in the case of MC1 and MC2 have a different effect on the low-frequency branches (I and II) of dispersion curves. From a comparison of the form of dispersion curves I and II in Fig. 4, *c* and Fig. 4, *e*, it can be seen that for the MC1 structure (see Fig. 1, *b*), there are practically no changes in the dispersion of I and II branches caused by reflection from the grooves on the film surface $z = d$ (Fig. 4, *c*). For the case of the MC2 structure, where the lattice of grooves is considered to be formed on the surface $z = 0$, on the contrary, replication, which is a consequence of reflections, takes place (Fig. 4, *e*). This dependence of the dispersion character of branches I, II on the choice of the film surface on which the periodic structure is formed should be related to the fact that branch I has the nature of „internal“ MSSW, and its fields are localized, mainly, in the region of several layers near $z = 0$. As a result, for MC1, where the lattice of grooves is formed near the surface $z = d$, the Bragg resonances in the dependences $f(k)$ and $S_{21,12}(f)$ for branch I in the framework of the used approach, are not observed.

For the structures MC1 and MC2, the modification of the $f(k)$ spectrum, associated with the appearance of two DER grids corresponding to the SWR modes in the film sections with thicknesses d and d^*, also differs. In the case of MC1, under the groove, the magnetization changes from 1700 G (at $z = 0$) to 1994.9 G (at $z = d^*$, $b = 60$ nm) or to 1969.8 G (for $z = d^*$, $b = 120$ nm). For MC2 — from 1725.1 G (at $z = b = 60$ nm) or from 1750.2 G (at $z = b = 120$ nm) to 2020 G (at $z = d$). As a result, the positions of both the DER grid and BRs turn out to be nonequivalent for MC1 and MC2. Besides, for MC1 the level of losses in the BR, as a whole, turns out to be higher than in the case of the MC2 structure (compare the values of ΔA at the BR frequencies in Fig. 4, *d* and *f*).

Part of the DER coincides with the position of BR, leading to absorption increasing at resonance. At $b = 60$ nm the changes in $f(k)$ and $S_{21,12}(f)$ associated with BR are less pronounced than at the resonance frequencies of MSSW and ESW (Fig. 4). However, the resulting BR demonstrate a level of damping similar to the BR in MC based on the YIG film with a uniform $4\pi M$ distribution and the same groove depth. At $b = 120$ nm, in the central region of the transmission zone, the damping value both in the DER and in the BR increases almost by two times.

4. Conclusion

The method of micromagnetic modeling is used to study the features of spin wave propagation in the YIG films of with nonuniformity across the thickness and in magnonic crystals based on them with a field and wave vector configuration corresponding to MSSW. It is shown that magnonic crystals based on the YIG film with a linear magnetization profile through the film thickness demonstrate a number of features. First, in the MSSW transmission band, a frequency range is formed in which the MSSW propagation is characterized not only by nonreciprocity, but also by unidirectionality, due to which there are no Bragg resonances in this range. Second, the signal damping in the region of the Bragg resonances exhibits nonreciprocity and can be additionally enhanced if it coincides with dipole-exchange resonances. And finally, the position of the Bragg and dipole-exchange resonances depends on the surface of the nonuniform film in which the magnonic crystal is formed.

Funding

This study was carried out within the framework of a state assignment and partially supported by the Russian Foundation for Basic Research (RFBR project No. 20-57-00008 Bel_A).

Conflict of interest

The authors declare that they have no conflict of interest.

References

[1] S.A. Nikitov, Ph. Tailhades, C.S. Tsai. J. Magn. Magn. Mater. **236**, *3*, 320 (2001).
[2] Yu.V. Gulyaev, S.A. Nikitov, L.V. Zhivotovsky, A.A. Klimov, F. Tayad, L. Presmanes, K. Bonin, Ch.S. Tsai, S.L. Vysotsky, Yu.A. Filimonov. Pis'ma v ZhETF **77**, *10*, 670 (2003) (in Russian).
[3] S.A. Nikitov, D.V. Kalyabin, I.V. Lisenkov, A.N. Slavin, Yu.N. Barabanenkov, S.A. Osokin, A.V. Sadovnikov, E.N. Beginin, M.A. Morozova, Yu.P. Sharaevsky, Yu.A. Filimonov, Yu.V. Khivintsev, S.L. Vysotsky, V.K. Sakharov, E.S. Pavlov. UFN **185**, *10*, 1099 (2015) (in Russian).
[4] M. Krawczyk, D. Grundler. J. Phys.: Condens. Matter **26**, *12*, 123202 (2014).
[5] A.V. Chumak, A.A. Serga, B. Hillebrands. J. Phys. D Appl. Phys. **50**, *24*, 244001 (2017).
[6] Yu.A. Ignatov, A.A. Klimov, S.A. Nikitov, V.I. Shcheglov. FTT **52**, *10*, 1950 (2010) (in Russian).
[7] A.N. Kuchko, M.L. Sokolovskii, V.V. Kruglyak. Physica B **370**, *1-4*, 73 (2005).
[8] Y. Filimonov, E. Pavlov, S. Vystostkii, S. Nikitov. Appl. Phys. Lett. **101**, 242408 (2012).
[9] T. Langner, D.A. Bozhko, S.A. Bunyaev, G.N. Kakazei, A.V. Chumak, A.A. Serga, B. Hillebrands, V.I. Vasyuchka. J. Phys. D Appl. Phys. **51**, *34*, 344002 (2018).

[10] S.L. Vysotsky, S.A. Nikitov, N.N. Novitsky, A.I. Stogniy, Yu.A. Filimonov. ZhTF **81**, *2*, 150 (2011) (in Russian).
[11] V.V. Kruglyak, A.N. Kuchko, V.I. Finokhin. FTT **46**, *5*, 842 (2004) (in Russian).
[12] S.M. Suturin, A.M. Korovin, V.E. Bursian, L.V. Lutsev, V. Bourobina, N.L. Yakovlev, M. Montecchi, L. Pasquali, V. Ukleev, A. Vorobiev, A. Devishvili, N.S. Sokolov. Phys. Rev. Mater. **2**, *10*, 104404 (2018).
[13] V.K. Sakharov, Y.V. Khivintsev, S.L. Vysotskii, A.I. Stognij, Y.A. Filimonov. IEEE Magn. Lett. **8**, 3704105 (2017).
[14] L.V. Lutsev, V.O. Shcherbakova, G.Ya. Fedorova. FTT **35**, *8*, 2208 (1993) (in Russian).
[15] L.V. Lutsev, Yu.M. Yakovlev. FTT **30**, *6*, 1675 (1988) (in Russian).
[16] Yu.V. Gulyaev, P.E. Zilberman, E.S. Sannikov, V.V. Tikhonov, A.V. Tolkachev. Pis'ma v ZhTF, **14**, *10*, 884 (1988) (in Russian).
[17] Yu.V. Gulyaev, P.E. Zilberman, A.G. Temiryazev. Pis'ma v ZhTF **21**, *19*, 27 (1995) (in Russian).
[18] P.E. Zilberman, A.G. Temiryazev, M.P. Tikhomirova. UFN **165**, *10*, 1219 (1995) (in Russian).
[19] Yu.A. Filimonov, G.T. Kazakov, S.L. Visotsky, B.P. Nam, A.S. He. J. Magn. Magn. Mater. **131**, *1-2*, 235 (1994).
[20] R.A. Gallardo, P. Alvarado-Seguel, T. Schneider, C. Gonzalez-Fuentes, A. Roldan-Molina, K. Lenz, J. Lindner, P. Landeros. New J. Phys. **21**, *3*, 033026 (2019).
[21] V.I. Zubkov, V.A. Epanechnikov. Pis'ma v ZhTF **23**, *11*, 1419 (1985) (in Russian).
[22] R.W. Damon, J.R. Eshbach. J. Phys. Chem. Solids **19**, *3-4*, 308 (1961).
[23] V.K. Sakharov. Cand. dis. Spin-volnovye vozbuzhdeniya v mikrostrukturakh na osnove polikristallicheskikh magnitnykh plenok. Izd-vo „Tekhno-Dekor“, Saratov (2021) (in Russian).
[24] M.J. Donahue, D.G. Porter. OOMMF user's guide. Interagency Report NIST 6376 (1999).
[25] M. Dvornik, Y. Au, V.V. Kruglyak. In: Magnonics. / Ed. S. Demokritov, A. Slavin. Springer, Berlin (2013). P. 101–115.
[26] E. Schlomann. J. Appl. Phys. **35**, *1*, 159 (1964).
[27] R.E. De Wames, T. Wolfram, J. Appl. Phys. **41**, *3*, 987 (1970).
[28] Yu.V. Gulyaev, A.S. Bugaev, P.E. Zilberman, I.A. Ignatiev, A.G. Konovalov, A.V. Lugovskoy, A.M. Mednikov, B.P. Nam, E.I. Nikolaev. Pis'ma v ZhETF **30**, *9*, 600 (1979) (in Russian).
[29] V.F. Dmitriev, B.A. Kalinikos. Izv.vuz. Ser. fiz. **31**, *11*, 24 (1988) (in Russian).
[30] M. Mruczkiewicz, E.S. Pavlov, S.L. Vysotsky, M. Krawczyk, Yu.A. Filimonov, S.A. Nikitov. Phys. Rev. B **90**, *17*, 174416 (2014).
[31] R.L. Carter, C.V. Smith, J.M. Owens. IEEE Trans. Magn. **16**, *5*, 1159 (1980).